



Ultrafiltration of municipal wastewater: study on fouling models and fouling mechanisms

J.L. Soler-Cabezas*, M. Torà-Grau, M.C. Vincent-Vela, J.A. Mendoza-Roca, F.J. Martínez-Francisco

Instituto de Seguridad Industrial, Radiofísica y Medio Ambiental, Universitat Politècnica de València, Camino de Vera s/n, 46022 Valencia, Spain, Tel. +34 96 387 70 00, ext. 76380; Fax: +34 96 387 76 39; emails: jsoca@isiryum.upv.es (J.L. Soler-Cabezas), mitogr@etsii.upv.es (M. Torà-Grau), mavinve@iqn.upv.es (M.C. Vincent-Vela), jamendoz@iqn.upv.es (J.A. Mendoza-Roca), framarfr@iqn.upv.es (F.J. Martínez-Francisco)

Received 15 July 2014; Accepted 22 September 2014

ABSTRACT

Ultrafiltration (UF) with hollow fiber membranes is a proven membrane technique that can achieve high water quality standards as a tertiary treatment in municipal wastewater treatment plants. However, UF has a major drawback, membrane fouling, which causes losses of productivity and increases operation costs. Thus, the aim of this work is to model membrane fouling in the UF of a secondary treatment effluent. The tests were carried out with a model wastewater solution that consisted of bovine serum albumin and dextran. Three different transmembrane pressures and three different crossflow velocities were tested. Several fouling models available in the literature, and new models proposed, were fitted to permeate flux decline experimental data. The models studied by other authors and considered in this study were: Hermia's models (complete, intermediate, standard pore blocking and gel layer) and Belfort's model. The new models proposed in this work were: modified Belfort's model, quadratic exponential model, logarithmic inversed model, double exponential model and tangent inversed model. The fitting accuracy of the models was determined in terms of the *R*-squared and standard deviation. The results showed that the model that had the higher fitting accuracy was the logarithmic inversed model. Among the Hermia's models, the model that had the higher fitting accuracy was the intermediate pore blocking model. Therefore, the predominant fouling mechanism was determined and it was the intermediate pore blocking model.

Keywords: Ultrafiltration; Fouling; Modeling; Hollow fiber; Simulated wastewater

1. Introduction

The conventional treatment of a municipal wastewater treatment plant (MWWTP) consists of a pre-

treatment, followed by a primary treatment (physico-chemical), a secondary treatment (activated sludge) and, depending on each case, a tertiary treatment.

The need for a tertiary treatment is due to the fact that the water quality resulting from a secondary treatment effluent (STE) could not be good enough for

*Corresponding author.

Presented at the IX Ibero-American Congress on Membrane Science and Technology (CITEM 2014), 25–28 May 2014, Santander, Spain

some applications, for example reuse in agriculture where disinfection is very important.

Ultrafiltration (UF) is a membrane technique suitable for a tertiary treatment [1,2] and can be applied to the reclamation of municipal wastewater [3,4]. In fact, UF achieves high quality standards [5] and disinfection [6–9]. Compared to conventional treatments, UF has some advantages: high permeate quality, no by-product generation, efficient, easy to operate, economically feasible, reduced membrane costs and energy consumption, low pressure, small footprint [6,10–13].

As reported in the literature, the best UF membranes available in order to treat a STE are hollow fiber (HF) membranes [5]. HF membranes have some advantages such as its large packing density [14], larger ratio of membrane area to unit volume, self-supporting and flexibility in the mode of operation [6].

The major problem of membrane UF is fouling [15]. Fouling causes permeate flux decline (this implies losses in productivity and lower plant availability [16]) [17], higher operating costs (as a consequence of higher energy costs [18]) and higher maintenance costs [16] (as consequence of lower membrane lifetime [15] and frequent membrane replacement).

It is important to minimize membrane fouling so that the process could be economically feasible [19]. For this reason, the scientific community has studied extensively membrane fouling and it is still studied since the fouling mechanisms are not completely understood [20,21] and further investigation is required. Particularly, membrane fouling of HF UF membranes is still an unresolved subject. The main difference between this study and the literature is the fact that the authors proposed some new empirical models that are not reported in the literature.

Due to the fact that the STE composition and concentration is variable with time, the use of model wastewater is useful to model UF membrane fouling.

In the STE wastewater, extracellular polymeric substances (EPS) are known to be the primarily responsible for membrane fouling in biological effluents [11]. EPS consist of polysaccharides, proteins, nucleic acids and humic substances [22]. However, the major components of EPS are protein and carbohydrates [23,24].

Thus, the tests were carried out using synthetic wastewater, that consisted of bovine serum albumin (BSA) and dextran, a protein and a carbohydrate, respectively. These compounds were studied by other authors. For example, Zator et al. [22] studied a mixture of BSA and dextran and Xiao et al. [25] worked with these compounds as model foulants.

Mathematical modeling of permeate flux decline is important so it can be useful to design, optimize and

control the filtration process [26]. In addition, mathematical modeling facilitates scaling up membrane systems and understanding membrane fouling [27]. In the literature there are some models (theoretical [28,29], empirical [30] and semi-empirical [31] models) available to attempt to predict permeate flux decline.

The aim of this study was to model HF membrane fouling in the UF of STE from a MWWTP.

2. Modeling

Flux decline vs. time data was fitted to some empirical and semi-empirical models, namely: Hermia's models adapted to crossflow filtration (complete, intermediate and standard pore blocking; gel layer), Belfort's model and other new models proposed in this work (modified Belfort's model, double exponential, tangent inversed, quadratic exponential and logarithmic inversed).

The fouling mechanisms can be determined in the case of semi-empirical models such as Hermia's models. However, the other models considered in this work are completely empirical. Therefore, the fouling mechanisms cannot be inferred and their parameters do not have physical meaning. Nevertheless, empirical models have the advantage of being very precise. In addition, theoretical models that achieve accurate prediction require at least one experimental parameter in order to predict permeate flux decline and their accuracy is lower than that of empirical models [32].

Model fitting was evaluated by means of the coefficient of determination (R^2) and standard deviation (SD).

The following permeate flux decline models were considered in this paper.

2.1. Hermia's models adapted to cross-flow filtration

These models are particular cases of the general equation Eq. 1, where "n" depends on the predominant fouling mechanism [33]: complete pore blocking model ($n=2$), intermediate pore blocking model ($n=1$), standard pore blocking model ($n=1.5$) and gel layer model ($n=0$).

$$-\frac{dJ_p}{dt} = K_{CF}(J_p - J_{pss})J_p^{2-n} \quad (1)$$

where J_p is the permeate flux at time "t", J_{pss} is the steady-state permeate flux and K_{CF} is a model constant.

Table 1 shows the equations associated to their respective models [34], obtained by integrating Eq. (1).

where K_c , K_i , K_s and K_{g1} are the characteristic constants of the complete pore blocking, the intermediate pore blocking, the standard pore blocking and the gel layer formation models, respectively. J_0 is the initial permeate flux.

According to Field et al. [33] and Vincent et al. [34], each Hermia’s model assumes the following hypotheses:

The complete pore blocking model assumes that pore sealing is the dominant blocking mechanism due to the fact that all solute that arrives at the membrane surface participates in blocking. No solute attaches onto a previously deposited solute on the membrane surface. The flux through the membrane pores that are not blocked remains constant, then the reduction in permeate flux is proportional to the reduction in membrane surface area.

The intermediate pore blocking model assumes that a membrane pore is not blocked necessarily by a solute and the probability of a solute to settle over a previously deposited solute is considered. The membrane surface that is not blocked diminishes with time and, with it, the probability of a solute to block a membrane pore.

The standard pore blocking model assumes that solutes are deposited within the membrane pores, then the pore volume is reduced with time. Some solutes are adsorbed instead of being only deposited over the internal surface of membrane pores.

The gel layer model assumes that solutes cannot enter inside the membrane pores. These solutes form a gel layer over the membrane surface. The resistance of this gel layer remains constant.

Experimental data fitting to the above mentioned models helps to infer the fouling mechanisms occurring during UF tests.

2.2. Belfort’s model

Mallubhotla and Belfort [30] proposed the following model, that is based on an exponential flux decline.

$$J(t) = J_0 \cdot \exp\left\{\frac{-t}{f(t)}\right\} \tag{6}$$

where “ f ” is a function of time. Belfort proposed this function to be linear.

$$f(t) = A_1 + A_2 \cdot t \tag{7}$$

where “ A_1 ” and “ A_2 ” are empirical constants.

2.3. New models proposed

All known functions can be classified in: algebraic (polynomial, rational functional, irrational), piecewise functions and transcendent (trigonometric, logarithm and exponential). Authors’ models are based on some of these functions.

The authors found some models that could represent or mimic the characteristic shape of the permeate flux decline. These models were obtained on the basis of their simplicity and their higher fitting accuracy to experimental data.

2.3.1. Modified Belfort’s model (quadratic)

In this model the Belfort’s function “ f ” is proposed to be a quadratic function instead of a linear function in order to improve the fitting of the model to the experimental data.

$$f(t) = B_1 + B_2 \cdot t + B_3 \cdot t^2 \tag{8}$$

where “ B_1 ”, “ B_2 ” and “ B_3 ” are empirical constants.

2.3.2. Tangent inversed model

In order to achieve a simple empirical model, trigonometric functions were selected as possible candidates. The inverse of the tangent function (between 0 and $\pi/2$ radians) seems to be similar in shape to the experimental permeate flux decline.

The authors tested the following empirical equation to model permeate flux decline.

$$J(t) = C_1 + \frac{C_2}{\tan(C_3 \cdot t + C_4)} \tag{9}$$

where “ C_1 ”, “ C_2 ”, “ C_3 ”, “ C_4 ” are empirical constants.

2.3.3. Quadratic exponential model

The inverse of the exponential function has similar trend to that of the experimental permeate flux decline.

The model proposed is based on the Hermia’s complete pore blocking model, however it considers two parameters instead of one in order to improve the model accuracy. The model equation is the following.

$$J(t) = J_{Pss} + (J_0 - J_{Pss}) \cdot e^{-(D_1 \cdot t + D_2 \cdot t^2)} \tag{10}$$

Table 1
Hemia's model equations

Model	Flux decline equation	Equations
Complete blocking	$J_p = J_{PSS} + (J_0 - J_{PSS}) \cdot e^{-K_s \cdot J_0 \cdot t}$	Eq. (2)
Intermediate blocking	$J_p = \frac{J_0 \cdot J_{PSS} \cdot e^{K_s \cdot J_{PSS} \cdot t}}{J_{PSS} + J_0 (e^{K_s \cdot J_{PSS} \cdot t} - 1)}$	Eq. (3)
Standard blocking	$J_p = \frac{J_0}{(1 + J_0^{1/2} \cdot K_s \cdot t)^2}$	Eq. (4)
Gel layer formation	$J_p = \frac{1}{2(-J_0 + e^{J_{PSS} \cdot K_{gl} \cdot t} \cdot J_0)} \cdot \left(-J_0 \cdot J_{PSS} + e^{J_{PSS} \cdot K_{gl} \cdot t} \cdot J_0 \cdot J_{PSS} - J_{PSS}^2 + \sqrt{4 \cdot J_0 \cdot (-J_0 + e^{J_{PSS} \cdot K_{gl} \cdot t} \cdot J_0) \cdot J_{PSS}^2 + (J_0 \cdot J_{PSS} - e^{J_{PSS} \cdot K_{gl} \cdot t} \cdot J_0 \cdot J_{PSS} + J_{PSS}^2)^2} \right)$	Eq. (5)

“D₁” and “D₂” are empirical constants.

2.3.4. Logarithmic inversed model

The inverse of the logarithmic function seems to be similar in shape to the experimental permeate flux decline.

The authors tested the following empirical equation to model permeate flux decline:

$$J(t) = E_1 + \frac{E_2}{\ln(E_3 \cdot t + E_4)} \tag{11}$$

where “E₁”, “E₂”, “E₃” and “E₄” are empirical constants.

2.3.5. Two exponential model

This model was developed considering two challenges: it should be simple and it should have enough parameters to achieve a high R² value.

$$J(t) = F_1 \cdot \frac{(F_2 + e^{F_3 \cdot t})}{(F_4 + e^{F_5 \cdot t})} \tag{12}$$

“F₁”, “F₂”, “F₃”, “F₄” and “F₅” are empirical constants. This model has a certain resemblance to another model proposed by Hasan et al. [35]. It must be noted that, inside the equation, the denominator must be higher than the numerator.

3. Materials and Methods

3.1. Wastewater characterization

A STE effluent from a MWWTP was characterized and the following parameters were measured: proteins and carbohydrates concentration, chemical oxygen demand (COD) and pH.

The COD was measured using the kit reference 1.14560.0001 and a thermoreactor model “TR300” both from Merck. The proteins concentration was determined by a MicroBCA assay (Bicinchoninic acid protein assay micro) from Applichem. The carbohydrates concentration was determined by the anthrone (9,10-dihydro-9-ketoanthracene) method (reagent from Panreac). The pH was measured using a Delta-Ohm pH-meter model HD2305.0.

3.2. Particle size distribution and Zeta-Potential

The particle size distribution (PSD) and Zeta-Potential was determined with a Zetasizer Nano-ZS 90 from Malvern that measures the particle size by laser diffraction.

3.3. Reagents

The following reagents were used in this study: BSA from Sigma–Aldrich and dextran from VWR International Ltd. The molecular weight of BSA and dextran reported was 66 KDa [36] and 250 KDa, respectively.

3.4. Model wastewater

Synthetic wastewater was used in the tests due to the fact that STE wastewater composition varies widely depending on the weather conditions, treatment system in the MWWTP, season of the year, hour of the day, and composition. A model wastewater was prepared at the laboratory mimicking the composition and fouling trend of the STE. (Muthukumaran et al. prepared a synthetic wastewater similar to the quality of the secondary treated wastewater [37].) This model wastewater consisted of tap water with BSA and dextran. Zator [22] and Kang Xiao [25] worked with BSA/dextran mixtures too. The model wastewater composition was selected so that the measured concentration of proteins and carbohydrates was similar to the average of different samples of the STE wastewater concentration. The simulated wastewater used in this work had the following composition: 15 mg/l of BSA and 5.5 mg/l of dextran.

3.5. UF HF membrane

A HF membrane was used for UF tests. The membrane used was a UFCM5 from Norit X-flow. The membrane properties are summarized in Table 2.

3.6. UF tests

Pilot plant UF tests were performed in a Norit X-flow T/RX-300 commercial pilot plant.

During the tests, the retentate and the permeate were both returned to the feed tank (total recirculation mode). The feed tank was stirred during the test. The temperature was set to 21 °C during the tests.

Table 2
Membrane properties

Membrane area	0.04 m ²
Hydraulic membrane diameter	1.5 mm
MWCO (molecular weight cut off)	200 KDa
Material	Polyethersulfone and polyvinylpyrrolidone
Configuration	Inside–out
Hydrophilic	Yes

Table 3
Operating conditions of the tests performed

Test Id.	TMP (MPa)	CFV (m/s)
SW1	0.10	0.50
SW2	0.10	0.75
SW3	0.10	1.00
SW4	0.15	0.50
SW5	0.15	0.75
SW6	0.15	1.00
SW7	0.20	0.50
SW8	0.20	0.75
SW9	0.20	1.00

The TMP was varied between 0.10 and 0.20 MPa and the CFV was varied in the range of 0.5–1 m/s. Three different levels of TMP and CFV were considered (Table 3), following an experimental design 3².

Low pressures were selected on the basis of some studies that report that the lower the TMP the lower membrane fouling [5,38]. A CFV of 1 m/s is within the range reported in the literature [38,39].

4. Results and discussion

4.1. Wastewater characterization

Table 4 shows the results on wastewater characterization. Protein and carbohydrate concentration values were used as reference to prepare a model wastewater that mimics the fouling trend of STE wastewater.

Table 4
Wastewater characterization

Parameter	Value
COD (mg/l)	38.9
Proteins (mg/l)	16.48
Carbohydrates (mg/l)	7.32
pH	7.11

4.2. Wastewater simulation

Table 5 shows the measured values of COD, proteins, carbohydrates concentration and pH of the model wastewater (15 mg/l of BSA and 5.5 mg/l of dextran). These values are similar to those of Table 4.

In Fig. 1 the normalized permeate flux (J_N) for STE, model wastewater, BSA and dextran is represented. Permeate flux has been normalized using Eq. (13).

$$J_N = J \cdot \frac{R_0}{R_m} \quad (13)$$

where “ J ” is permeate flux decline, “ R_0 ” is the membrane resistance of the original membrane and “ R_m ” is the resistance of the membrane before the test.

The results show that the simulated wastewater mimics the fouling trend of the STE wastewater (Fig. 1). In Fig. 1, the individual effect of BSA and dextran on membrane fouling can be observed.

BSA produces more fouling in the initial flux decline than dextran. The reason could be the internal pore blocking caused by BSA molecules that have not formed aggregates, what implies penetration of these molecules into the pores. As a consequence, the initial

Table 5
Simulated wastewater characterization

Parameter	Value
COD (mg/l)	27
Proteins (mg/l)	17.3
Carbohydrates (mg/l)	7.6
pH	6.16

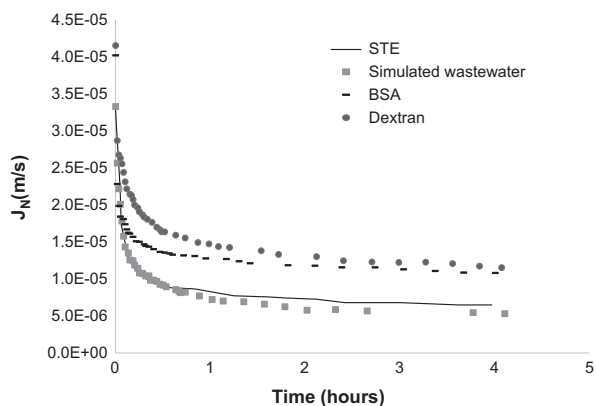


Fig. 1. Permeate flux decline for STE, simulated wastewater, BSA and dextran (0.07 MPa and 1 m/s).

flux decline in the experiment with BSA was higher than in the experiment with dextran, whose molecular size is slightly higher than membrane pores; thereby molecules will enter membrane pores at a lower extent.

4.3. Particle size distribution

Although the BSA molecular weight (66 KDa) is lower than the molecular weight cut-off of the membrane (200 KDa) and its nominal particle diameter (around 6–12 nm [22]) is lower than membrane pore size (21 nm), BSA is partially retained in the UF tests.

In Fig. 2, the PSD shows two peaks for the BSA, one at 2.943 nm and another at 244.6 nm. The second one is the peak with higher intensity. This suggests that BSA tends to form agglomerates, as reported by [40,41]. Thus, BSA is partially retained in the UF tests.

4.4. Model fitting

The experimental permeate flux decline data was fitted to each fouling model considered in this work using non-linear regression numeric data algorithms.

The software used in this regression were MathCad[®] 14 and Excel[®]. Specifically, the built-in “genfit” function of MathCad that implements the Levenberg–Marquardt algorithm and, on the other hand, the Solver of Excel that implements the GRG2 (Generalized Reduced Gradient) algorithm.

As mentioned in Section 2, the fitting accuracy of the model to the experimental data was determined by means of the R^2 and SD values. However, as explained in [42] by Gu, not always a higher value of R^2 implies a better fitting. As an example, in the case of the quadratic exponential model, the value of R^2 for SW7 (0.72) is higher than the value of R^2 for SW6 (0.59) (Table 7) despite the fact that the fitting is—visually—worse in the case of SW7 which has a higher R^2 . Permeate flux decline for these two tests can be seen in Figs. 3 and 4.

Tables 6 and 7 show the measure of fit of the models to experimental data in terms of R^2 for the tests performed with simulated wastewater. Tables 8 and 9 show the corresponding SD.

As reported by [42,43], it is important to note that R^2 values can only be compared among different models for same experimental data.

Among the Hermia’s models, the model that fitted the best to the experimental results (considering both R^2 and SD values) was the intermediate pore blocking model except in the cases of test SW2 and SW6. For these tests the model that fitted the best was gel layer

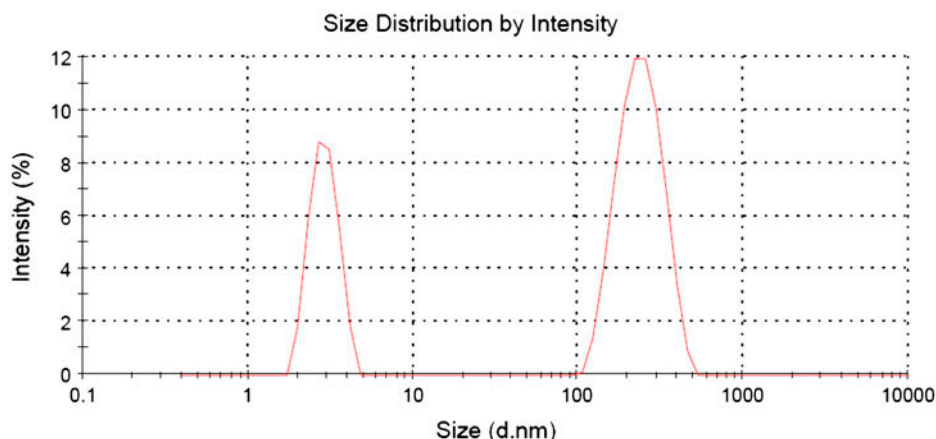
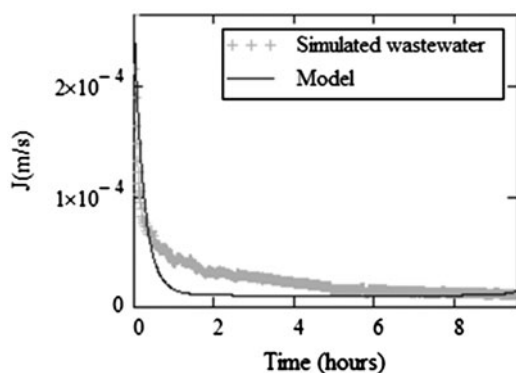
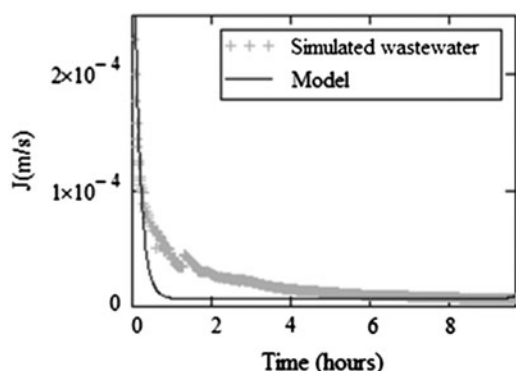


Fig. 2. PSD of BSA.

Fig. 3. Permeate flux decline for test SW6 and quadratic exponential model ($R^2 = 59\%$).Fig. 4. Permeate flux decline for test SW7 and quadratic exponential model ($R^2 = 72\%$).

model. However, the difference between the values of R^2 and SD for these two models is not significant since the relative error in the determination of experimental permeate flux is lower than 8.72%. This error was calculated according to Daufin [44,45].

One of the hypothesis of the intermediate pore blocking model was that not every molecule arriving at the membrane surface necessarily blocks a membrane pore. This can be explained considering the particle size of BSA and dextran and the molecular weight cut-off (MWCO) of the membrane. Dextran particle diameter is about 21.32 nm [46], very similar to the pore size of the membrane (21 nm). In addition, dextran is slightly deformable. Therefore some dextran molecules may not block the membrane, instead they pass through it.

On the other hand, as it can be seen in Fig. 2, the PSD of BSA shows two peaks: 2.943 and 244.6 nm (agglomerates diameter size). Considering that the membrane pore size is 21 nm, only part of BSA molecules may pass through the membrane. Indeed, the BSA rejection is about 44%. The rejected molecules are BSA aggregates.

Another assumption of the intermediate pore blocking model is that molecules are allowed to settle on each other. This is consistent with the fact that the membrane is slightly negatively charged, the BSA molecules are negatively charged and the dextran molecules are neutral. The measured Zeta-Potential of the simulated wastewater was -15.3 mV and the Zeta-Potential of the membrane at the same pH was around -15 mV. Thus, there is an electrical repulsion, what favours a reduction in the speed at which the final permeate flux is achieved [47]. Dextran can be deposited on the membrane due to its neutral charge. For BSA there are two possibilities: (1) when a BSA molecule arrives at the membrane, and no dextran

Table 6
R² values (part I)

Test Id.	Model				
	Complete blocking	Intermediate blocking	Standard blocking	Gel layer	Belfort
SW1	0.73	0.94	0.43	0.94	0.97
SW2	0.80	0.93	0.26	0.94	0.93
SW3	0.79	0.96	0.47	0.92	0.98
SW4	0.76	0.96	0.65	0.90	0.97
SW5	0.78	0.95	0.48	0.92	0.98
SW6	0.57	0.90	0.38	0.95	0.92
SW7	0.71	0.96	0.75	0.88	0.94
SW8	0.80	0.98	0.66	0.89	0.97
SW9	0.79	0.98	0.83	0.83	0.96

Table 7
R² values (part II)

Test Id.	Model				
	Modified Belfort	Double exponential	Tangent (inversed)	Quadratic exponential	Logarithmic (inversed)
SW1	0.99	0.99	0.99	0.75	0.99
SW2	0.98	0.94	0.99	0.85	0.98
SW3	0.99	0.99	0.99	0.81	0.99
SW4	0.99	1.00	0.99	0.78	1.00
SW5	0.99	0.99	0.99	0.81	0.99
SW6	0.99	0.98	0.98	0.59	0.99
SW7	0.97	0.99	0.99	0.72	1.00
SW8	0.99	0.99	1.00	0.83	1.00
SW9	0.98	0.99	0.99	0.81	0.99

Table 8
Standard deviation (part I)

Test Id.	Model				
	Complete blocking	Intermediate blocking	Standard blocking	Gel layer	Belfort
SW1	9.06×10^{-6}	4.31×10^{-6}	1.32×10^{-5}	4.35×10^{-6}	3.06×10^{-6}
SW2	4.09×10^{-6}	2.47×10^{-6}	7.95×10^{-6}	2.29×10^{-6}	2.37×10^{-6}
SW3	8.74×10^{-6}	3.87×10^{-6}	1.40×10^{-5}	5.48×10^{-6}	2.75×10^{-6}
SW4	1.18×10^{-5}	4.65×10^{-6}	1.44×10^{-5}	7.52×10^{-6}	4.26×10^{-6}
SW5	8.39×10^{-6}	3.99×10^{-6}	1.28×10^{-5}	4.89×10^{-6}	2.80×10^{-6}
SW6	1.53×10^{-5}	7.46×10^{-6}	1.83×10^{-5}	5.44×10^{-6}	6.45×10^{-6}
SW7	1.85×10^{-5}	6.56×10^{-6}	1.70×10^{-5}	1.20×10^{-5}	8.53×10^{-6}
SW8	9.32×10^{-6}	3.09×10^{-6}	1.22×10^{-5}	6.90×10^{-6}	3.37×10^{-6}
SW9	1.24×10^{-5}	3.88×10^{-6}	1.11×10^{-5}	1.12×10^{-5}	5.65×10^{-6}

molecule is deposited on the membrane, the BSA is repelled by the membrane due to the fact that the BSA and the membrane have identical charges and they repel each other. (2) when a BSA molecule arrives at the membrane, and a dextran molecule is deposited previously on the membrane, the BSA molecule is attached onto the dextran molecule due to the fact that

the dextran molecule is neutral. Note that the first possibility for BSA also explains the previous hypothesis: not all molecules arriving at the membrane cause pore blocking.

The Hermia's standard pore blocking model has significantly lower R-squared values compared with other Hermia's models. This fact suggests that the

Table 9
Standard deviation (part II)

Test Id.	Model				
	Modified Belfort	Double exponential	Tangent (inversed)	Quadratic exponential	Logarithmic (inversed)
SW1	1.60×10^{-6}	1.93×10^{-6}	1.74×10^{-6}	8.69×10^{-6}	1.46×10^{-6}
SW2	1.20×10^{-6}	2.23×10^{-6}	1.13×10^{-6}	3.58×10^{-6}	1.24×10^{-6}
SW3	1.38×10^{-6}	1.40×10^{-6}	1.50×10^{-6}	8.28×10^{-6}	1.63×10^{-6}
SW4	1.87×10^{-6}	1.62×10^{-6}	1.85×10^{-6}	1.13×10^{-5}	1.23×10^{-6}
SW5	1.54×10^{-6}	1.52×10^{-6}	1.39×10^{-6}	7.83×10^{-6}	1.33×10^{-6}
SW6	2.39×10^{-6}	3.21×10^{-6}	3.41×10^{-6}	1.49×10^{-5}	1.72×10^{-6}
SW7	6.11×10^{-6}	3.35×10^{-6}	4.05×10^{-6}	1.83×10^{-5}	1.94×10^{-6}
SW8	2.22×10^{-6}	1.95×10^{-6}	1.42×10^{-6}	8.73×10^{-6}	1.12×10^{-6}
SW9	3.91×10^{-6}	3.15×10^{-6}	2.84×10^{-6}	1.19×10^{-5}	2.45×10^{-6}

hypotheses of this model are not complied, maybe due to the fact that this kind of fouling is related to particles with a smaller diameter than the membrane pore size which are able to cause internal pore blocking [48]. In addition, the fitting accuracy of the standard pore blocking model obtained in this work is so much lower than that found in the literature [49–53]. These authors worked with the following feed solutions: skimmed coconut milk, succinic acid fermentation broth, palm oil–oleic acid–glycerin, palm oil mill effluent, glycerin-rich solutions, respectively.

In the case of the Belfort's model, the R -squared values are higher than the values obtained for the Hermia's models. On the other hand, the R -squared values obtained for the Belfort's model (0.92 min–0.98 max) are similar to those obtained by Mallubhotla and Belfort (0.94 min–0.99 max) during microfiltration of yeast [34].

For the models proposed by the authors, the R -squared values are higher than the values obtained for Hermia's models and Belfort's model, with the exception of the quadratic exponential model. Even in this case, the R -squared values are higher than those obtained for Hermia's standard pore blocking model.

Table 10
Best model per test depending on the R -squared and SD values

Test Id	Best model
SW1	Logarithmic (inversed)
SW2	Tangent (inversed)
SW3	Belfort quadratic
SW4	Logarithmic (inversed)
SW5	Logarithmic (inversed)
SW6	Logarithmic (inversed)
SW7	Logarithmic (inversed)
SW8	Logarithmic (inversed)
SW9	Logarithmic (inversed)

Table 10 shows the model that fits the best to each test, considering both SD values and R^2 values simultaneously.

According to Table 10, the model that fits the best to the experimental data was the logarithmic (inversed) model, except in the cases of tests SW2 and SW3. For those tests, the best model was the tangent inversed and the Belfort quadratic model, respectively.

The difference in the predominant mechanism in the cases of SW2 and SW3 can be attributed to the relative error in the determination of permeate flux as previously explained.

5. Conclusions

In most of the tests performed, the model that fitted the best to the experimental data was the logarithmic (inversed) model. However, this model, due to its empirical nature, does not explain the fouling mechanisms during the UF of the model foulants. The only model considered in this work that is able to explain the fouling mechanisms is the Hermia's model. Then, according to the fitting results of Hermia's models, the predominant fouling mechanism was intermediate pore blocking. This fact was explained in this work considering the molecular size of the foulants with respect to the membrane pore size and the electrical charges of the foulants and the membrane.

Acknowledgements

The authors wish to gratefully acknowledge the financial support of the *Generalitat Valenciana* through the project "Ayudas para la realización de proyectos I+D para grupos de investigación emergentes GV/2013".

Nomenclature

MWCO	—	molecular weight cut-off
TMP	—	transmembrane pressure, MPa
CFV	—	cross-flow velocity, m/s
SEM	—	scanning electron microscopy
STE	—	secondary treatment effluent
SW	—	synthetic wastewater
J	—	permeate flux, m/s
J_0	—	initial permeate flux, m/s
J_N	—	dimensionless permeate flux
J_{PSS}	—	steady-state permeate flux
R^2	—	coefficient of determination
SD	—	standard deviation
K_{CF}	—	cross-flow model parameter
K_c	—	complete blocking model characteristic parameter, m^{-1}
K_i	—	intermediate blocking model characteristic parameter, m^{-1}
K_s	—	standard blocking model characteristic parameter, $s^{-0.5} \cdot m^{-0.5}$
K_{gl}	—	gel layer (cake formation) model characteristic parameter, $s \cdot m^{-2}$
A_i	—	model constant parameter
B_i	—	model constant parameter
C_i	—	model constant parameter
D_i	—	model constant parameter
E_i	—	model constant parameter

References

- [1] V. Gadani, R. Irwin, V. Mandra, Ultrafiltration as a tertiary treatment: Joint research program on membranes, *Desalination* 106 (1996) 47–53.
- [2] J. Illueca-Muñoz, J.A. Mendoza-Roca, A. Iborra-Clar, A. Bes-Piá, V. Fajardo-Montañana, F.J. Martínez-Francisco, I. Bernácer-Bonora, Study of different alternatives of tertiary treatments for wastewater reclamation to optimize the water quality for irrigation reuse, *Desalination* 222 (2008) 222–229.
- [3] Metcalf & Eddy, *Water Reuse: Issues, Technologies and Applications*, AECOM, McGraw-Hill, New York, NY, 2007.
- [4] S. Muthukumaran, J.V. Jegatheesan, K. Baskaran, Comparison of fouling mechanisms in low-pressure membrane (MF/UF) filtration of secondary effluent, *Desalin. Water Treat.* 52 (2014) 650–662.
- [5] S. Delgado, F. Díaz, L. Vera, R. Díaz, S. Elmaleh, Modelling hollow-fibre ultrafiltration of biologically treated wastewater with and without gas sparging, *J. Membr. Sci.* 228 (2004) 55–63.
- [6] J.J. Qin, M.H. Oo, H. Lee, R. Kolkman, Dead-end ultrafiltration for pretreatment of RO in reclamation of municipal wastewater effluent, *J. Membr. Sci.* 243 (2004) 107–113.
- [7] K. Konieczny, Disinfection of surface and ground waters with polymeric ultrafiltration membranes, *Desalination* 119 (1998) 251–258.
- [8] S.S. Madaeni, A.G. Fane, G.S. Grohmann, Virus removal from water and wastewater using membranes, *J. Membr. Sci.* 102 (1995) 65–75.
- [9] J.M. Arnal-Arnal, M. Sancho-Fernández, G. Martín-Verdú, J. Lora-García, Design of a membrane facility for water potabilization and its application to Third World countries, *Desalination* 137 (2001) 63–69.
- [10] J. Arévalo, G. Garralón, F. Plaza, B. Moreno, J. Pérez, M.A. Gómez, Wastewater reuse after treatment by tertiary ultrafiltration and a membrane bioreactor (MBR): A comparative study, *Desalination* 243 (2009) 32–41.
- [11] K. Katsoufidou, S.G. Yiantsios, A.J. Karabelas, An experimental study of UF membrane fouling by humic acid and sodium alginate solutions: The effect of backwashing on flux recovery, *Desalination* 220 (2008) 214–227.
- [12] S. Muthukumaran, D.A. Nguyen, K. Baskaran, Performance evaluation of different ultrafiltration membranes for the reclamation and reuse of secondary effluent, *Desalination* 279 (2011) 383–389.
- [13] R.K. Henderson, N. Subhi, A. Antony, S.J. Khan, K.R. Murphy, G.L. Leslie, Vicki Chen, P. Le-Clech, Evaluation of effluent organic matter fouling in ultrafiltration treatment using advanced organic characterisation techniques, *J. Membr. Sci.* 382 (2011) 50–59.
- [14] D. Xiao, W. Li, S. Chou, R. Wang, C.Y. Tang, A modeling investigation on optimizing the design of forward osmosis hollow fiber modules, *J. Membr. Sci.* 392–393 (2012) 76–87.
- [15] Y. Kaya, H. Barlas, S. Arayici, Evaluation of fouling mechanisms in the nanofiltration of solutions with high anionic and nonionic surfactant contents using a resistance-in-series model, *J. Membr. Sci.* 367 (2011) 45–54.
- [16] M. Amin Saad, Early discovery of RO membrane fouling and real-time monitoring of plant performance for optimizing cost of water, *Desalination* 165 (2004) 183–191.
- [17] C.H. Yu, L.C. Fang, S.K. Lateef, C.H. Wu, C.F. Lin, Enzymatic treatment for controlling irreversible membrane fouling in cross-flow humic acid-fed ultrafiltration, *J. Hazard. Mater.* 177 (2010) 1153–1158.
- [18] W. Gao, H. Liang, J. Ma, M. Han, Z.L. Chen, Z.S. Han, G.B. Li, Membrane fouling control in ultrafiltration technology for drinking water production: A review, *Desalination* 272 (2011) 1–8.
- [19] A. Jayalakshmi, S. Rajesh, D. Mohan, Fouling propensity and separation efficiency of epoxidated polyethersulfone incorporated cellulose acetate ultrafiltration membrane in the retention of proteins, *Appl. Surf. Sci.* 258 (2012) 9770–9781.
- [20] F. Qu, H. Liang, Z. Wang, H. Wang, H. Yu, G. Li, Ultrafiltration membrane fouling by extracellular organic matters (EOM) of *Microcystis aeruginosa* in stationary phase: Influences of interfacial characteristics of foulants and fouling mechanisms, *Water Res.* 46 (2012) 1490–1500.
- [21] C. Wang, Q. Li, H. Tang, D. Yan, W. Zhou, J. Xing, Y. Wan, Membrane fouling mechanism in ultrafiltration of succinic acid fermentation broth, *Bioresour. Technol.* 116 (2012) 366–371.
- [22] M. Zator, M. Ferrando, F. López, C. Güell, Membrane fouling characterization by confocal microscopy during filtration of BSA/dextran mixtures, *J. Membr. Sci.* 301 (2007) 57–66.

- [23] G.P. Sheng, H.Q. Yu, X.Y. Li, Extracellular polymeric substances (EPS) of microbial aggregates in biological wastewater treatment systems: A review, *Biotechnol. Adv.* 28 (2010) 882–894.
- [24] S.T. Nguyen, F.A. Roddick, Chemical cleaning of ultrafiltration membrane fouled by an activated sludge effluent, *Desalin. Water Treat.* 34 (2011) 94–99.
- [25] K. Xiao, X. Wang, X. Huang, T.D. Waite, X. Wen, Analysis of polysaccharide, protein and humic acid retention by microfiltration membranes using Thomas' dynamic adsorption model, *J. Membr. Sci.* 342(1–2) (2009) 22–34.
- [26] C. Suh, S. Lee, J. Cho, Investigation of the effects of membrane fouling control strategies with the integrated membrane bioreactor model, *J. Membr. Sci.* 429 (2013) 268–281.
- [27] C. Duclos-Orsello, W. Li, C.C. Ho, A three mechanism model to describe fouling of microfiltration membranes, *J. Membr. Sci.* 280 (2006) 856–866.
- [28] R.H. Davis, Modeling of fouling of crossflow microfiltration membranes, *Sep. Purif. Methods* 21 (1992) 75–126.
- [29] S. Bhattacharjee, P.K. Bhattacharya, Flux decline behaviour with low molecular weight solutes during ultrafiltration in an unstirred batch cell, *J. Membr. Sci.* 72 (1992) 149–161.
- [30] H. Mallubhotla, G. Belfort, Semiempirical modeling of cross-flow microfiltration with periodic reverse filtration, *Ind. Eng. Chem. Res.* 35 (1996) 2920–2928.
- [31] J. Hermia, Constant pressure blocking filtration laws—Application to power-law non-Newtonian fluids, *Trans. Inst. Chem. Eng.* 60 (1982) 183–187.
- [32] A. Salahi, M. Abbasi, T. Mohammadi, Permeate flux decline during UF of oily wastewater: Experimental and modeling, *Desalination* 251 (2010) 153–160.
- [33] R.W. Field, D. Wu, J.A. Howell, B.B. Gupta, Critical flux concept for microfiltration fouling, *J. Membr. Sci.* 100 (1995) 259–272.
- [34] M.C. Vincent-Vela, S. Álvarez-Blanco, J. Lora-García, E. Bergantiños-Rodríguez, Analysis of membrane pore blocking models adapted to crossflow ultrafiltration in the ultrafiltration of PEG, *Chem. Eng. J.* 149 (2009) 232–241.
- [35] A. Hasan, C.R. Peluso, T.S. Hull, J. Fieschko, S.G. Chatterjee, A surface-renewal model of cross-flow microfiltration, *Braz. J. Chem. Eng.* 30 (2013) 167–186.
- [36] W.S. Ang, M. Elimelech, Protein (BSA) fouling of reverse osmosis membranes: Implications for wastewater reclamation, *J. Membr. Sci.* 296 (2007) 83–92.
- [37] S. Muthukumar, K. Baskaran, Comparison of the performance of ceramic microfiltration and ultrafiltration membranes in the reclamation and reuse of secondary wastewater, *Desalin. Water Treat.* 52 (2014) 670–677.
- [38] F. Tasselli, A. Cassano, E. Drioli, Ultrafiltration of kiwi-fruit juice using modified poly(ether ether ketone) hollow fibre membranes, *Sep. Purif. Technol.* 57 (2007) 94–102.
- [39] T. Chung, J. Qin, J. Gu, Effect of shear rate within the spinneret on morphology, separation performance and mechanical properties of ultrafiltration polyethersulfone hollow fiber membranes, *Chem. Eng. Sci.* 55 (2000) 1077–1091.
- [40] T. Swaminathan, M. Chaudhuri, K.K. Sirkar, Anomalous flux behavior in initial time stirred protein ultrafiltration through partially permeable membranes, *J. Appl. Polym. Sci.* 24 (1979) 1581–1585.
- [41] A.L. Ahmad, N.A.H. Hairul, Protein-membrane interactions in forced-flow electrophoresis of protein solutions: Effect of initial pH and initial ionic strength, *Sep. Purif. Technol.* 66 (2009) 273–278.
- [42] Z. Gu, Across-sample incomparability of R2s and additional evidence on value relevance changes over time, *J. Bus. Finance Acc.* 34(7–8) (2007) 1073–1098.
- [43] M.C. Vincent, S. Álvarez, J. Lora, E. Bergantiños, Analysis of membrane pore blocking models applied to the ultrafiltration of PEG, *Sep. Purif. Technol.* 62 (2008) 489–498.
- [44] G. Daufin, U. Merin, F.L. Kerhervé, J.P. Labbé, A. Quémerais, C. Bousser, Cleaning of inorganic membranes after whey and milk ultrafiltration, *Biotechnol. Bioeng.* 38 (1991) 82–89.
- [45] G. Daufin, U. Merin, F.L. Kerhervé, J.P. Labbé, A. Quémerais, C. Bousser, Efficiency of cleaning agents for an inorganic membrane after milk ultrafiltration, *J. Dairy Res.* 59 (1992) 29–38.
- [46] A. Morão, J.C. Nunes, F. Sousa, M.T.P. Amorim, I.C. Escobar, J.A. Queiroz, Development of a model for membrane filtration of long and flexible macromolecules: Application to predict dextran and linear DNA rejections in ultrafiltration, *J. Membr. Sci.* 336 (2009) 61–70.
- [47] M. Ouammou, N. Tijani, J.I. Calvo, C. Velasco, A. Martín, F. Martínez, F. Tejerina, A. Hernández, Flux decay in protein microfiltration through charged membranes as a function of pH, *Colloids Surf., A* 298 (2007) 267–273.
- [48] T. Mohammadi, M. Kazemimoghadam, M. Saadabadi, Modeling of membrane fouling and flux decline in reverse osmosis during separation of oil in water emulsions, *Desalination* 157 (2003) 369–375.
- [49] C.Y. Ng, A.W. Mohammad, L.Y. Ng, J.M. Jahim, Membrane fouling mechanisms during ultrafiltration of skimmed coconut milk, *J. Food Eng.* 142 (2014) 190–200.
- [50] C. Wang, Q. Li, H. Tang, D. Yan, W. Zhou, J. Xing, Y. Wan, Membrane fouling mechanism in ultrafiltration of succinic acid fermentation broth, *Bioresour. Technol.* 116 (2012) 366–371.
- [51] S.K. Mah, C.K. Chuah, W.P. Cathie Lee, S.P. Chai, Ultrafiltration of palm oil-oleic acid-glycerin solutions: Fouling mechanism identification, fouling mechanism analysis and membrane characterizations, *Sep. Purif. Technol.* 98 (2012) 419–431.
- [52] M. Said, A. Ahmad, A.W. Mohammad, M.T.M. Nor, S.R. Sheikh Abdullah, Blocking mechanism of PES membrane during ultrafiltration of POME, *J. Ind. Eng. Chem.* (2014), doi: [10.1016/j.jiec.2014.02.023](https://doi.org/10.1016/j.jiec.2014.02.023).
- [53] I.N.H.M. Amin, A.W. Mohammad, M. Markom, L.C. Peng, N. Hilal, Analysis of deposition mechanism during ultrafiltration of glycerin-rich solutions, *Desalination* 261 (2010) 313–320.